MICRO-CRACK DETECTION OF SOLAR CELLS FEATURING ADAPTIVE ANISOTROPIC DIFFUSION FILTER AND SEMI-SUPERVISED SUPPORT VECTOR LEARNING

by

SAID AMIRUL ANWAR B AB HAMID @ AB MAJID

Thesis submitted in fulfillment of the requirements
for the degree of
Doctor of Philosophy

August 2014

ACKNOWLEDGMENT

First and foremost, my deepest gratitude is to my supervisor, Professor Dr. Mohd Zaid Abdullah, who provided me valuable advice, tremendous support and guidance for my study and research. I also would like to thank the administrative and supportive staff of School of Electrical and Electronic Engineering for their instant assistance whenever needed. I would like to thank my colleagues and friends who provided encouragements and precious help. Thanks also to my parents who have been incredibly supportive especially during difficult periods. Finally, sincere gratitude goes to my beloved wife, son and daughter who accompanied me throughout my study.

TABLE OF CONTENTS

ACKNOWLEDGMENT ii

TABLE OF CONTENTS iii

LIST OF FIGURES vii

LIST OF TABLES xi

LIST OF ABBREVIATIONS xii

LIST OF SYMBOLS xiii

LIST OF ALGORITHMS xv

ABSTRAK xvi

ABSTRACT xviii

CHAPTER 1: INTRODUCTION **1**

1.1 Motivation 1

1.2 Difficulties and challenges 3

1.3 Research objectives 12

1.4 Research scope 12

1.5 Thesis outline 13

CHAPTER 2: LITERATURE REVIEW **14**

2.1 Image Processing 14

2.1.1 Preprocessing 15

2.1.2 Anisotropic diffusion 16

2.1.3 Segmentation 26

2.2 Shape representation 30

2.2.1 Angular radial transform 33
2.3 Machine learning 36
2.3.1 Support vector machines 38
2.3.1.1 One-class SVM 44
2.3.2 Problem of imbalanced dataset 46
2.3.2.1 Fuzzy SVM 48
2.3.2.2 Other approaches 50
2.3.3 Semi-supervised learning 52
2.3.4 Support vector clustering 56
2.3.4.1 Cluster assignment 61
2.3.5 Novelty detection 63
2.4 Crack detection algorithms 66
2.5 Summary 71

CHAPTER 3: METHODOLOGY **72**

3.1 Dataset 73
3.2 Image segmentation 74
3.2.1 Proposed algorithm 77
3.2.1.1 Image filtering 77
3.2.1.2 Anisotropic diffusion filter 81
3.2.1.3 Two-stage thresholding technique 87
3.2.2 Accuracy measures 93
3.3 Shape analysis 94
3.3.1 Principal component analysis 95
3.3.2 Separability measure 96

3.4 Supervised learning 97
3.4.1 Confusion matrix 98
3.4.2 Geometric mean 100
3.5 Semi-supervised learning 101
3.5.1 Proposed algorithm 105
3.5.2 Performance measures 111
3.5.3 Rand index 113
3.6 Summary 114

CHAPTER 4: EXPERIMENTAL RESULTS **115**

4.1 Image processing 116
4.1.1 Image filtering 116
4.1.2 Image enhancement 118
4.1.3 Image segmentation 123
4.1.4 Parameters selection 129
4.2 Shape analysis 133
4.3 Classifiers analysis 137
4.3.1 Supervised learning 138
4.3.2 Semi-supervised learning 141
4.4 Summary 149

CHAPTER 5: CONCLUSIONS AND FUTURE WORKS **151**

5.1 Concluding remarks 151
5.2 Future works 155
5.3 Summary 156

REFERENCES 157

APPENDIX A: SUPPLEMENTARY SEGMENTATION RESULTS 171

APPENDIX B: EXAMPLE OF SHAPE DESCRIPTOR SPECTRUMS 179

APPENDIX C: LIST OF PUBLICATIONS 183

LIST OF FIGURES

1.1 Multicrystalline solar cells. An optical image of (a) cell; EL image of (b) intact cell, (c) cracked cell. Micro-crack is marked by an arrow in (c). 2

1.2 Electroluminescence image of multicrystalline solar cell showing grain boundaries, micro-crack, dark areas, bus-bars and metal fingers contact. 4

1.3 Examples of micro-cracks and dark regions. (a) various types, sizes and shapes of micro-cracks; (b) various formations of dark regions. . . 5

2.1 Laplacian neighbors of pixel (m, n). 17

2.2 Example of image preprocessing. (a) original circuit image; (b) filtered with Gaussian low pass filter mask of size 5 and standard deviation 3; (c) edge detection using Canny detector; (d) processed using anisotropic diffusion filter with $K = 3$ and $t = 32$. 19

2.3 Example of shape, projections into first quadrant and ART spectrum. (a) original flower shape; (b) projections of (a); (c) ART spectrum of (a). 37

2.4 Example of SVM learning. (a) maximal margin; (b) soft margin. Training data in (b) is mapped using RBF kernel function. + and $*$ represent positive and negative class respectively, ○ is SV, solid line is a hyperplane and dotted line is the margin. 43

2.5 Example of hyperplane and support vectors of OCSVM trained with different value of ν. Training data is mapped using RBF kernel function with $\sigma = 2$. • and ○ represent training data and support vectors respectively and solid line is a hyperplane. 46

2.6 Example of training dataset used in different machine learning approach. (a) supervised; (b) unsupervised; (c) semi-supervised. △, + and • is a first class, second class and unlabeled data respectively. . 53

2.7 Example of SVC training showing (a) original unlabeled data, (b), (c) and (d) are training results for different value of σ. All SVC training are performed with $\nu = 0.1$. • is unlabeled data point, + is enclosed point, ○ and $*$ is SV and BSV respectively and solid line is a hypersphere. 60

3.1 Block diagram of the micro-crack detection algorithm. 73

3.2 Flowchart of the proposed image segmentation algorithm. 76

3.3 Multicrystalline solar cell images. (a) cracked cell; (b) close-up view of (a); (c) good cell; (d) close-up view of (c). The dashed circle in (a) shows the location of the micro-crack. 78

3.4 Characteristics of micro-crack pixels. (a) close-up view of micro-crack pixels; (b) gray level profile; (c) gradient level profile. The dashed line in (a) marks the location of the scan line. 79

3.5 Three-dimensional plot of a custom filter function H. 80

3.6 Diffusion coefficient comparing original and proposed modifications. All responses are plotted with $K = 64$. $c_1(s)$, $c_2(s)$ and $c_3(s)$ refers to Equations (2.8), (2.9) and (3.5) respectively. 82

3.7 Plot of the response of the proposed diffusion coefficient with different values of s and g. 83

3.8 Image filtering comparing proposed and conventional anisotropic diffusion filters. (a) original synthetic image; (b) proposed filter with $a = 0.1$ and $\epsilon = 128$; (c) and (d) original filter with $K = 100$ and $K = 5$ respectively; (e)-(h) are plots of gray levels profile of (a)-(d) respectively. $t = 100$ for all processing. Original diffusion filter is based on Equation (2.9). 84

3.9 An enhancement using image subtraction technique. (a) difference image; (b) gray levels profile of (a). Image in (a) is normalized to [0,255] to show details. 86

3.10 Histogram plot of the difference image, I_Δ. 88

3.11 Flowchart describing distribution of the dataset, training mode and testing mode. (a) training mode; (b) testing mode. 98

3.12 Confusion matrix for two class classification problem 99

3.13 Flowchart of semi-supervised learning for new class detection algorithm. 103

4.1 EL image filtering in the frequency domain. (a) original image; (b) Fourier spectrum; (c) filtered image. The dashed circle in (a) and (c) shows the location of the micro-crack. Filtering is performed with $w = 6$, $r = 10$ and $\sigma = 12$. 117

4.2 Close-up views and gray level profiles of the image before and after filtering. (a) before; (b) after; (c) and (d) are plots of gray levels profile of (a) and (b) respectively. The dashed line in (a) and (b) marks the location of the scan line. 117

4.3 Results of filtering in the frequency domain for EL images of cracked solar cells. (a) full-size image; (b) filtered image of (a); (c) and (d) are close-up views of the cracked region in (a) and (b) respectively. 119

4.4 Micro-crack pixel enhancement using the proposed anisotropic diffusion filter. (a) filtered image; (b) diffused image obtained with $a = 1$, $\epsilon = 128$ and $t = 4$; (c) difference image; (d), (e) and (f) are plots of gray level profile of (a), (b) and (c) respectively. The dashed line in (a) and (b) marks the location of the scan line. Image in (c) is normalized to [0,255] to show details. 120

4.5 Results of micro-crack pixels enhancement for selected EL images of cracked solar cells. (a) diffused image; (b) difference image obtained from the subtraction of (a) from the image in Figures 4.3(d). 121

4.6 Results of micro-crack pixels enhancement using existing anisotropic diffusion filters. (a) filter proposed by Chao and Tsai (2006) with $K_0 = 2$; (b) filter proposed by Chao and Tsai (2010) with $K_0 = 80$; (c) filter proposed by Tsai *et al.* (2010) with $K = 64$. 122

4.7 Results of two-stage thresholding technique using difference image in Figure 4.5(b) as input. (a) seed image; (b) target image; (c) reconstructed image and (d) final segmented image. 124

4.8 Image segmentation results comparing the proposed and standard segmentation techniques. (a) ground truth images; (b) proposed technique; (c) FIR; (d) Canny hysteresis; (e) LoG filter; (f) Otsu's thresholding; (g) Sobel edge detector. 125

4.9 F-measure comparing proposed and standard segmentation techniques. 129

4.10 Effect of parameter a on difference images. (a) 0.1; (b) 1; (c) 10. All images are normalized to [0,255] to show details. Experiment is performed using $\epsilon = 128$ and $t = 4$. 130

4.11 The effect of the number of iteration on accuracy measure. Images are preprocessed with $\epsilon = 128$ and $a = 1$. 131

4.12 Effect of threshold k_U on the final binary images. (a) 0.5; (b) 1.5; (c) 2.5. Images are segmented with $\epsilon = 128$, $a = 1$ and $t = 4$. 132

4.13 Example of ART spectrums for different types of shapes. (a) micro-crack shapes; (b) spectrum of (a); (c) arbitrary shapes; (d) spectrum of (c). 134

4.14 PCA of shape features comparing ART with other shape descriptor. (a) ART; (b) FD; (c) FPDFD; (d) GFD; (e) RCF. +, • and ▲ represent micro-crack shapes, arbitrary shapes and centroid of each group respectively. 136

4.15 The separability measures comparing the ART, FD, FPDFD, GFD and RCF shape descriptors. 137

4.16 Performance measures of new class detection algorithm for the working set. (a) correct rate; (b) misclassification error rate; (c) false prediction error rate; (d) overall error rate. Dashed horizontal line represents overall correct rate and dashed vertical line marks the point where new class is detected. 144

4.17 The details of the computational time of the proposed micro-crack detection algorithm. 149

A.1 Image segmentation results comparing the proposed and the standard image segmentation technique. (a) ground truth images; (b) proposed technique; (c) FIR; (d) Canny hysteresis; (e) LoG filter; (f) Otsu's thresholding; (g) Sobel edge detector. 171

B.1 Example of Fourier descriptor (FD) spectrums for different types of shapes. (a) micro-crack shape; (b) spectrum of (a); (c) arbitrary shapes; (d) spectrum of (c). 179

B.2 Example of farthest point distance Fourier descriptor (FPDFD) spectrums for different types of shapes. (a) micro-crack shape; (b) spectrum of (a); (c) arbitrary shapes; (d) spectrum of (c). 180

B.3 Example of generic Fourier descriptor (GFD) spectrums for different types of shapes. (a) micro-crack shape; (b) spectrum of (a); (c) arbitrary shapes; (d) spectrum of (c). 181

B.4 Example of Radon composite features (RCF) spectrums for different types of shapes. (a) micro-crack shape; (b) spectrum of (a); (c) arbitrary shapes; (d) spectrum of (c). 182

LIST OF TABLES

3.1 The number of EL images of good and cracked solar cells 74

3.2 Distribution of EL images of good and cracked solar cells in the dataset used in machine learning 74

4.1 Completeness and correctness measures of the segmentation results. . 128

4.2 The details of shape features for training set based on ART. 137

4.3 The classification results of the testing set. 138

4.4 The classification results of shape features of the testing set. 140

4.5 Distribution of cells and shapes in the training and working sets. . . . 142

4.6 The details of the parameters and results for the working set. 145

4.7 Confusion matrix of prediction results before the new class is detected. 146

4.8 Confusion matrix of prediction results after the new class is detected. . 147

4.9 The classification results for micro-crack detection using the proposed semi-supervised learning. 147

A.1 Completeness, correctness and F-measure indices of the segmentation results. 177

LIST OF ABBREVIATIONS

νSVM	ν(New) Support Vector Machines
kNN	k Nearest Neighbor
ART	Angular Radial Transform
BSV	Bounded Support Vector
CED	Coherence Enhance Diffusion
CG	Connected Graph
DFT	Discrete Fourier Transform
EL	Electroluminescence
FD	Fourier Descriptor
FIR	Fourier image reconstruction
FPDFD	Farthest Point Distance Fourier Descriptor
FSVM	Fuzzy Support Vector Machines
GFD	Generic Fourier Descriptor
KKT	Karush-Kuhn-Tucker
LDA	Linear Discriminant Analysis
LoG	Laplacian of Gaussian
LSSVM	Least-Square Support Vector Machines
MAD	Median Absolute Deviation
MAT	Multistage Adaptive Thresholding
MPEG	Moving Picture Experts Group
MR	Magnetic Resonance
OCSVM	One-Class Support Vector Machines
PCA	Principal Component Analysis
PV	Photovoltaic
QDA	Quadratic Discriminant Analysis
QP	Quadratic Programming
RBF	Radial Basis Function
RCF	Radon Composite Features
S^3VM	Semi-supervised Support Vector Machines
SMO	Sequential Minimal Optimization
SNR	Signal to Noise Ratio
SOM	Self Organizing Map
SPM	Statistical Parametric Map
SV	Support Vector
SVC	Support Vector Clustering
SVDD	Support Vector Domain Description
SVM	Support Vector Machines

LIST OF SYMBOLS

a	Gradient of the sigmoidal ramp
b	Bias
c	Diffusion coefficient
e	Error rate
f	Discrimination function
g	Sigmoid transfer function
h, k	User defined parameter
m, n	Spatial domain coordinate
p	Angular order
q	Radial order
r	Radius
s	Magnitude of gradient
t	Iteration
u, v	Frequency domain coordinate
w	Width
y	Data label
A	Angular part
B	Binary image
C	Penalty parameter
D	Distance measure
G	Gaussian function
H	Frequency domain filter
I	Image
K	Edge stopping threshold
R	Radial part
R_γ	Dynamic range of standard deviation
S	Binary connected component, shape
V	Basis function
$\mathbf{c}$	Centre, centroid
$\mathbf{w}$	Weight vector
$\mathbf{x}$	Training data
$\mathbf{A}$	Adjacency matrix
$\mathbf{C}$	Covariance matrix
$\mathbf{E}$	Eigenvectors
$\mathbf{U}$	Traced gray levels
$\mathbf{\Lambda}$	Eigenvalues
ℓ	Number of elements
α	Lagrangian multiplier
δ	Line step point
ϵ	Sigmoidal centre mapping
γ	Standard deviation
η	Dimension
κ	Kernel
λ	Fuzzy membership

μ	Mean
ν, ρ	νSVM parameters
∇	Gradient
ϕ	Non-linear map
σ	Gaussian function parameter
τ	Threshold
ξ	Cluster size
ϖ	Maximum iteration
ζ	Slack variable
Γ	Separability measure
Ω	Domain
Ψ	Structuring element
Υ	Angular radial transform
$\mathcal{F}$	Discrete Fourier transform
$\mathcal{H}$	Heaviside function
$\mathcal{L}$	Class label
$\mathcal{M}$	Misclassification stack
$\mathcal{O}$	One-class classifier set
$\mathcal{R}$	Rand index
$\mathcal{S}$	Working set
$\mathcal{T}$	Predicted label
$\mathcal{U}$	Cluster index
$\mathcal{V}$	Cluster label
$\mathcal{X}$	Training set
$\mathcal{Y}$	Training set label
$\mathfrak{R}$	Real number
$\mathfrak{I}$	Imaginary number
$\cap$	Morphological intersection
$\oplus$	Morphological dilation
$\langle \cdot \rangle$	Inner product
$\lvert \cdot \rvert$	Magnitude
$\lVert \cdot \rVert$	Norm
div	Divergent operator
max	Maximize
min	Minimize
s.t.	Subject to
sign	Sign

LIST OF ALGORITHMS

3.1 Prediction phase 108

3.2 Detection phase 110

PENGESANAN KERETAKAN-MIKRO SEL SOLAR DENGAN MEMPERSEMBAHKAN PENAPIS TAK ISOTROPI SUAI RESAPAN DAN PEMBELAJARAN SOKONGAN VEKTOR SEPARUH-DISELIA

ABSTRAK

Dalam tesis ini, satu aplikasi berasaskan penglihatan mesin untuk mengesan keretakan-mikro dalam imej elektropendarkilau (EL) sel solar dibentangkan. Pengesanan ini adalah masalah yang mencabar berikutan kerumitan sifat tekstural dan ketakhomogenan latar belakang imej EL. Walaubagaimanapun, kecacatan keretakan-mikro mempamerkan beberapa ciri-ciri unik seperti kecerunan yang tinggi dan paras-kelabu yang rendah. Ciri-ciri ini bersama-sama dengan ciri bentuk keretakan-mikro digunakan dalam membangunkan algoritma pengesanan. Dalam penyelidikan ini, satu algoritma pemprosesan imej yang mempersembahkan penapis tak isotropi suai resapan dan teknik segmentasi berdasarkan pengambangan dua-peringkat telah dicadangkan. Hasil algoritma ini telah menunjukkan keputusan segmentasi yang sangat tepat berbanding dengan kaedah piawai yang lain. Berdasarkan ukuran ketepatan, kaedah yang dicadangkan mencapai F-measure 0.0821. Ciri-ciri imej tempatan seperti perwakilan bentuk komponen bersambung binari diekstrak dan digunakan dalam pembelajaran mesin untuk membezakan antara sel-sel solar retak dengan yang baik. Ia telah dapat dibuktikan bahawa perihal bentuk penjelmaan sudut jejarian (ART) telah menghasilkan set ciri-ciri yang paling diskriminatif dan boleh pisah yang mencatatkan nilai pengukuran kebolehpisahan 8.36. Pembelajaran mesin berdasarkan pendekatan separuh-diselia dengan keupayaan mengesan kelas baru dalam sejumlah besar data tidak berlabel telah dicadangkan. Dalam pendekatan pembelajaran ini, pengelas mesin sokongan vektor satu-kelas (OCSVM) dilatih dengan sejumlah kecil data yang dilabel manakala data tidak berlabel selebihnya telah digunakan

sebagai set kerja. Algoritma penggugusan sokongan vektor (SVC) telah digunakan untuk memeriksa dan menganalisis data yang tidak terkelas bagi mengesan data kelas baru. Dalam kes pengesanan keretakan-mikro sel-sel solar, algoritma separuh-diselia mengatasi pengelas diselia konvensional dan mencatatkan markah tertinggi bagi ketentuan, kejituan dan min geometri masing-masing 89.46%, 86.62% dan 85.85%. Tambahan pula, algoritma ini dapat menemui kelas baru sel-sel retak dan seterusnya meningkatkan keupayaan proses membuat keputusan secara keseluruhan. Pendekatan pembelajaran separuh-diselia yang dicadangkan didapati telah mengatasi kekurangan pengelas diselia konvensional dalam mengenal kategori baru data dan ini membawa kepada peningkatan dalam kecekapan klasifikasi.

MICRO-CRACK DETECTION OF SOLAR CELLS FEATURING ADAPTIVE ANISOTROPIC DIFFUSION FILTER AND SEMI-SUPERVISED SUPPORT VECTOR LEARNING

ABSTRACT

In this thesis, a machine vision-based application for detecting micro-crack in an electroluminescence (EL) image of solar cell is presented. The detection is a very challenging problem due to the complexity of the textural properties and background inhomogeneity of EL images. Nevertheless, the micro-crack defect exhibits some unique properties such as high in gradient and low gray-levels. These properties together with the shape feature of the micro-crack are used in developing the detection algorithm. In this work, an image processing algorithm featuring an adaptive anisotropic diffusion filter and a segmentation technique based on two-stage thresholding is proposed. The outcomes of this algorithm have demonstrated a highly accurate segmentation results compared to other standard methods. Based on the accuracy measure, the proposed methods achieve the highest F-measure of 0.0821. The local image features such as shape representation of the binary connected components are extracted and used in the machine learning to distinguish between cracked and good solar cells. It is discovered that an angular radial transform (ART) shape descriptor has produced the most discriminative and separable set of features which registered the value of separability measure of 8.36. The machine learning based on semi-supervised approach with the capability of detecting new class in the large number of unlabeled data is proposed. In this learning approach, the one-class support vector machine (OCSVM) classifiers are trained with a small number of labeled data while the remaining unlabeled data is used as working set. The support vector clustering (SVC) algorithm is employed to examine and analyze the misclassified data

points to detect the new class data. In the case of micro-crack detection of solar cells, the semi-supervised algorithm outperformed conventional supervised classifiers and scores the highest specificity, accuracy and geometric means of 89.46%, 86.62% and 85.85% respectively. Furthermore, this algorithm is able to discover new class of cracked cells and subsequently improve the ability of the overall decision making process. The proposed semi-supervised learning approach is found to have overcome the limitation of the conventional supervised classifiers in recognizing the new category of data and this leads to a further improvement in the classification efficiency.

CHAPTER 1

INTRODUCTION

1.1 Motivation

Photovoltaic (PV) industry is rapidly growing and expanding in order to meet the world's demand for renewable energy. Solar cells, being the major component in the PV module, are also increased in demands. Despite many types of solar cells in the market, crystalline silicon is the dominant technology used in the PV industries. Crystalline silicon solar cells can be in the form of monocrystalline and multicrystalline cells. Multicrystalline solar cells differ from monocrystalline because several types of silicon crystal are used in the process of producing wafer ingots whereas the latter only grows from single crystal. In addition, multicrystalline silicon is generally more popular for solar cell applications because it is more economical and cost effective to use in the production of the PV module. According to recent statistics, the growth rate of the solar PV module reached a record high in 2011, generating more than US$93 billion in revenue with multicrystalline cells constituting more than 50% of the world production (Solarbuzz, 2012).

One of the technological problems during the production of the PV module is the cells breakage due to micro-cracks. This type of defect has a dimension smaller than 30μm which is entirely invisible to the naked eyes (Chiou *et al.*, 2011). Hence, the micro-crack defect can only be visualized electronically like using a special approach such as electroluminescence (EL) technique (Fuyuki & Kitiyanan, 2009). Example of EL image of intact and cracked multicrystalline solar cells are shown in Figures 1.1(b)

(a) (b) (c)

Figure 1.1: Multicrystalline solar cells. An optical image of (a) cell; EL image of (b) intact cell, (c) cracked cell. Micro-crack is marked by an arrow in (c).

and (c) respectively. Clearly from Figure 1.1(c), micro-crack is visually observable. This is not possible from an optical image of solar cell such as in Figure 1.1(a). The presence of cracked cells in PV module increases the risk of its breakdown after a certain ageing (Köntges *et al.*, 2011). This is because, due to ageing and temperature variations, the micro-crack can propagate and interrupting the electrical network in the cells which can lead to failure (Zimmermann, 2006). Hence, it is important to have high-quality, defect-free cells in the production of PV modules.

In the recent years, there is an increasing trend in the use of machine vision in the industry and manufacturing sectors. Typical tasks of machine vision in the industrial vision inspection system are: image acquisition, image processing, feature extraction and decision making (Malamas *et al.*, 2003). The use of machine vision in industrial automation gives better solutions as it helps to increase productivity and quality through consistent, accurate and fast inspection. On contrary, the inspection by human experts sometimes degraded due to fatigue and discrepancies. Although many operations in the PV industry have been automated, the inspection and grading processes continue to be manual or semi-manual efforts. In this case, it is due to the lack of image processing and artificial intelligent algorithms which are suitable and

accurate in solving the inspection tasks involved. Inevitably, the problem of detecting micro-crack defects in solar cells also exhibit similar circumstances.

Therefore, there is a research prospective in the field of machine vision to solve the problem of micro-crack detection in solar cell. Motivated by the aforesaid situation, this thesis presents the methods and techniques for detecting micro-crack defects in the EL image of multicrystalline solar cell. This work integrates an image processing and machine learning platform toward its application in the micro-crack inspection. It addresses an image processing technique based on adaptive anisotropic diffusion filter and its application on EL images. Additionally, this work examines a local feature extraction method for shape analysis namely angular radial transform (ART). Further in this thesis, a machine learning and classification based on semi-supervised support vector learning is investigates. Finally, this work also examines the classification based on supervised support vector machines (SVM).

1.2 Difficulties and challenges

Electroluminescence (EL) imaging technique provides useful information about the electrical and material properties of solar cells (Fuyuki *et al.*, 2007; Fuyuki & Kitiyanan, 2009). This technique requires the cells to be in forward biased condition, emitting the radiations ranging from 950 to 1250nm which is then captured by near infrared camera. Emission intensity is dependent on the density of defects in the silicon, with fewer defects resulting in more emitted photons. In general the EL does not require an illumination and image acquisition must take place in the dark room. Among the advantages of this technique is that the image can be captured relatively fast; only in a few seconds per cell and it is more precise than the conventional

scanning method (Fuyuki & Kitiyanan, 2009). Furthermore, EL produces better spatial resolution images which make it a preferable imaging technique for micro-crack detection of solar cells (Breitenstein *et al.*, 2011). In addition, EL imaging setup is relatively cheaper and the instrumentation can easily be integrated into machine automation for an on-line inspection and control.

Figure 1.2 shows an example of EL image of multicrystalline solar cell highlighting few of its important texture characteristics. In this figure, solar cell image is an 8-bit gray scale measuring 1178×1178 pixels in size. As seen in Figure 1.2, crystal grains and dark regions are formed from intrinsic structures like dislocation clusters and grain boundaries. These formations of unpredictable intrinsic deficiency contributed to the inhomogeneity in the EL image. Distinguishing micro-crack pixels from the heterogeneous background is a very challenging procedure because the gray scale values of these two areas are not significantly different. The presence of other defects such as broken fingers and crystal impurities complicates the problem.

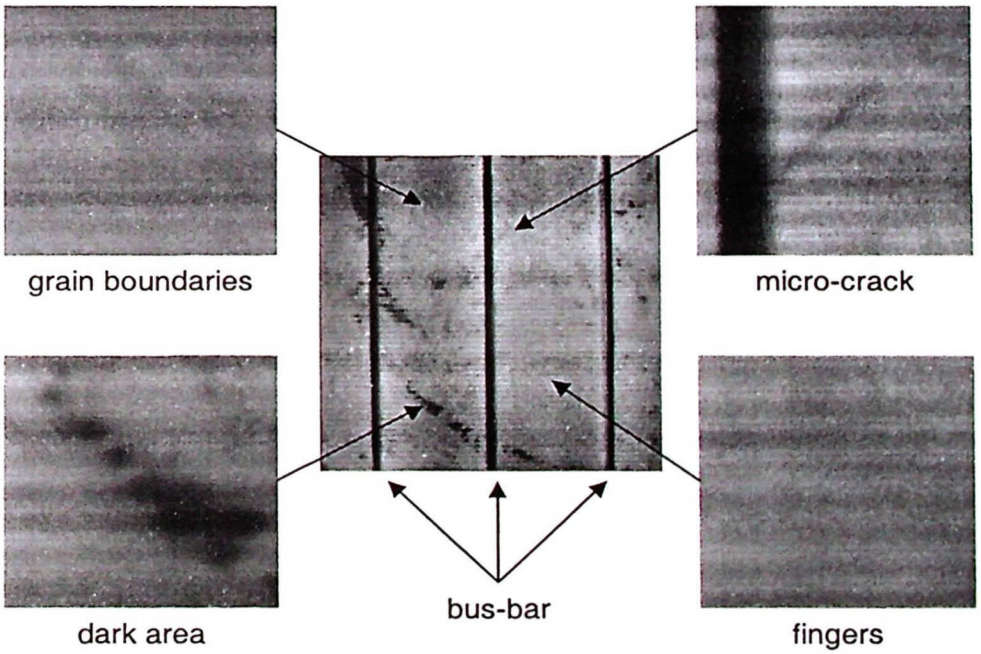

Figure 1.2: Electroluminescence image of multicrystalline solar cell showing grain boundaries, micro-crack, dark areas, bus-bars and metal fingers contact.

As seen in Figure 1.2, the EL images also contain standard technological features, such as fingers (horizontal lines) that are periodic in nature and perpendicular to the bus-bar (thicker vertical lines). The presence of these standard features directly affects the micro-crack analysis. In spite of these difficulties, the identification is still possible because the micro-crack pixels tend to appear in the form of strong lines with a low-intensity and a high gradient. Other examples of defected solar cells containing various types and shapes of micro-cracks are shown in Figure 1.3.

The micro-crack pixels appear in the form of a line or an intersection of lines forming a star-like artifact as depicted in Figure 1.3(a). In practice there are various types of shapes and sizes of micro-cracks in solar cell depending on how they are formed. For example a line shaped micro-crack is caused by scratches occurred during cell fabrication (Wen & Yin, 2012). This type of defect can also be due to wafer sawing or laser cutting, which propagates and causes the detachment or internal breakage of the grainy materials within the solar cells (Belyaev *et al.*, 2006). In contrast, star-shaped micro-crack is formed due to a sharp point impact which induces several line cracks with a tendency to cross each other (Demant *et al.*, 2011; Köntges *et al.*, 2013).

For comparison, Figure 1.3(b) shows examples of intact region of the solar cells

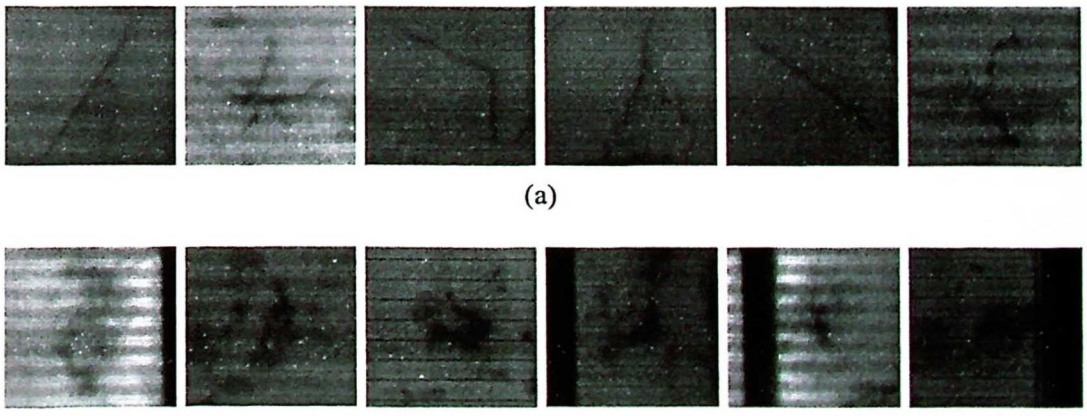

(a)

(b)

Figure 1.3: Examples of micro-cracks and dark regions. (a) various types, sizes and shapes of micro-cracks; (b) various formations of dark regions.

highlighting the presence of dark regions having arbitrary shapes and sizes. They are formed by an aggregate of dislocation clusters or grainy materials, resembling dark shaped areas when visualized under the EL illumination. As seen from this figure, the presence of many dark areas or regions in both good and defected samples makes a micro-crack inspection an extremely difficult process. However, a close examination of Figure 1.3(a) reveals that micro-crack pixels exhibit unique shapes or patterns compared to dark regions even though they have same gray scale values.

The difficulties in detecting micro-crack in EL image of solar cell have imposed a challenging task to the machine vision application. To date, there are few studies related to this field that use EL image for defect detection in solar cell. For example, the defect detection methods based on global image representation approach (Bastari *et al.*, 2010; Tsai *et al.*, 2013). In these methods, the EL images are represented by an extracted feature vectors. These vectors are used later in the decision making process to classify between good and defected cells. Although these methods are generally successful in detecting defected solar cell, they exhibit weakness such as inability to recognize the types of the defect. This is due to the limitations of a globally extracted feature where it is unable to acquire the presence of diminutive details such as micro-crack pixels. In the other approach, the subdivided image is processed in the spectral domain using Fourier transformation technique (Tsai *et al.*, 2012). The frequency spectrums are analyzed using a Hough transform-based line detector to detect the presence of a micro-crack defect. However, the dependency of this approach on a line detector only produces good detection of micro-crack pixels which are geometrically simple like a straight line. As a result, this approach demonstrates limitation as there are other forms of micro-crack that needs to be considered as shown in Figure 1.3(a).

Several key challenges in detecting micro-crack defect in EL images of solar cell are identified. First challenge is an enhancement of micro-crack pixels through image processing. Typically, image processing consists of preprocessing and segmentation procedures (Sonka *et al.*, 2008). In preprocessing, an image is usually processed in spatial or frequency domain. However, in some cases, preprocessing can be done in both spatial and frequency domain simultaneously or in cascading mode. Main aim of preprocessing is to enhance the desired (micro-crack) pixels or parts of the image while suppressing the unwanted pixels (noises). Edge detection method is an example of preprocessing technique in spatial domain. On the other hand, a filtering process performed on the Fourier spectrum is an example of preprocessing in the frequency domain. Subsequently, in segmentation procedure, the image is further processed and divided into several parts. Thresholding is a common technique used in the segmentation process. Generally, this technique divides the image into two parts namely object and background.

As evident from Figures 1.2 and 1.3(a), the difficulties in enhancing micro-crack pixels cannot be addressed using simple filtering or edge detection methods. Consideration has to be made to the textural properties of the EL images as well as the characteristics of the micro-crack pixels. For example, a use of low pass filter will reduce the presence of high frequency noises but unfortunately it also distorts the micro-crack pixels. Meanwhile, the convolution with edge detector masks will yield high and low gradients at the edges and micro-crack pixels respectively. The result is that the produced image contains two lines representing the edges of the micro-crack. Alternatively, there is a filtering technique referred to as anisotropic diffusion filter (Perona & Malik, 1990). This technique belongs to the scale-space image filtering

category where an input image is iteratively convolved with a filter over a certain period of time. The main advantages of the anisotropic diffusion filter is its ability to smooth specific section of the image while preserving the important edges (Catté *et al.*, 1992). For any pixel in the image, this filter uses the gradient information determined between this pixel and its Laplacian neighborhoods as a deciding factor on whether to smooth or to retain the gray value. From the perspective of edge detection, this filter produces a significantly better output compared to the state-of-art edge detection method (Weickert, 1997). Since then, anisotropic diffusion filter have evolved and used in many applications where the problem of filtering and detecting edges are required simultaneously.

Further in image processing, few important considerations have to be accounted including the task of suppressing the effect of the noisy pixels such as periodical interruptions by metal fingers and non-uniformity of the background luminescence. Additionally, the enhancement of the micro-crack pixels requires a filtering technique that is able to highlight specific pixels. In this case, the pixels that have low intensity in gray scale and high gradient. Subsequently, an accurate image segmentation procedure is highly desired in order to divide the preprocessed image into meaningful partitions. Accurate in this context refers to the precision of the thresholding technique in isolating micro-crack pixels and at the same time minimizing the presence of other artifacts.

The second challenge is an implementation of feature extraction procedure. In the view of machine vision application, this procedure usually preceded by image processing. Through feature extraction, the quantitative useful information from the segmented image is extracted and mapped to feature space where it will be used later in decision making. The selection of feature extraction technique depends on the

applications or problems in hand. In the case of EL image of solar cell, a visually distinct feature between micro-crack pixels and other defects is their patterns or shapes. This can be clearly observed from Figure 1.3. As discussed earlier, the global image feature extraction method will not be able to acquire the details of the micro-crack and its patterns effectively. Therefore, the local approach of representing these shapes has to be explored. In general, it is difficult to extract a very good feature that represents pattern or shape effectively (Zhang & Lu, 2004). This is contributed by the limitations of the shape descriptors. Hence, this imposes a challenge in the feature extraction procedure in this works. For that reason, an implementation of proper technique in extracting these valuable features from the segmented images is highly desired.

In machine vision application, decision making is the final procedure and it comprises of a classification task. There are two approaches of classification that are commonly used namely unsupervised and supervised learning. In unsupervised approach, the classifier learns without the training data. This approach uses the unlabeled data to establish the parameterized structures. An example of unsupervised learning is data clustering. On the contrary, a supervised approach requires training data in the learning step. In this case, the training data are all labeled. Next step in supervised learning approach is predicting the label for the newly unseen data. One of the examples of supervised learning approach is the classification using a standard SVM algorithm (Vapnik, 1998; Cristianini & Shawe-Taylor, 2000). Among the advantages of SVM is its ability to yield better classification results even in the case of only small number of training data is used (Shao & Lunetta, 2012). In addition, the time taken to train SVM is relatively faster since this technique is less computationally intensive compared to other standard methods (Moavenian & Khorrami, 2010). On

the other hand, there is another approach in machine learning research known as semi-supervised learning (Chapelle *et al.*, 2006). In this approach, the learning step uses both labeled and unlabeled data. Semi-supervised learning addresses the issue where there is only a small number of labeled data available in the learning step as compared to a large number of unlabeled data (Zhu, 2008). The unlabeled data is subsequently classified and the results are used to update the decision boundary of the initial classifier to produce better classification capability.

Most of the existing classification task assumes the number of points in each of target class is equally distributed. However, this is not usually the case. In reality, there are classification problems involved a highly imbalanced dataset. The difficulties in obtaining samples for a particular class of data probably due to the limitation of time, its existence or cost could cause the inequality in the dataset. Typically, for the dataset of this kind, the number of points in the majority class outnumbered the minority class by a very considerable ratio. This condition leads to a bias prediction of the testing points where the majority class will have better accuracy compared to the minority class (Blagus & Lusa, 2010). In dealing with this problem, the common approach is resampling of the training data or modifying the classification algorithm (Lin & Chen, 2012). The resampling technique aims to equalize the number of points in each class through under-sampling or up-sampling the majority or minority class. On the other hand, a more technical approach is a modification to the classification algorithm in order to compensate the problem of bias prediction internally.

Another important issue in the classification task is novelty detection. This problem sometimes referred to as anomaly or outlier detection. In a typical novelty detection algorithm, the decision boundary is established from the training data in

the learning step. This data is assumed as a normal or target class data. A new testing point is considered as an outlier if it lies outside the decision boundary. Thus, a group of outliers is treated as one new class of abnormal data. In this case, the problem of novelty detection becomes a one-class classification problem. Most of the existing novelty detection algorithms belong to this category (Khan & Madden, 2010). However, there are possibilities that the outliers belong to a few unknown classes. By taking into consideration of these odds, it becomes a novel or new class detection problem (Masud *et al.*, 2011). The difficulties in solving this problem lie in the analysis of the outliers. It involves recognition of the consistent structure that possibly exists among the outliers toward a formation of a new class.

In relation to the primary concerns of this study, the occurrence of the micro-crack in the solar cells may exhibit various unpredictable formations of shapes and patterns. Furthermore, it is impossible to obtain EL images of cracked solar cells that contain every possible pattern of micro-crack. Therefore, there is a possibility that the training data used to train the classifier do not contain sufficient samples that represent certain class of data. If trained with this kind of dataset, the existing supervised classification approach is unable to recognize the new data which do not belong to any of the classes learned and thus, this new sample will be wrongly classified. Therefore, this drawback imposes a challenge to the machine learning algorithm in the decision making procedure of the micro-crack inspection system. Hence, the machine learning approach with the ability to recognize and detect new class of data is necessary to overcome this shortcoming.

1.3 Research objectives

In this research, the solution to the problem of micro-crack detection of multicrystalline solar cells is presented. The framework of this study is focused on this application and the efforts are emphasized in solving the problem through the integration of image processing and machine learning platform. Therefore, the primary objectives of this research are stated as follows:

i. To develop an adaptive anisotropic diffusion filter for image preprocessing.

ii. To develop a multi-stage image thresholding technique.

iii. To develop a semi-supervised learning algorithm based on support vector machines and clustering for novel class detection.

In addition to the primary objectives, this research will also focus on secondary objectives as follows:

i. To investigate the effectiveness of angular radial transforms descriptor for shape representation.

ii. To compare the performance of the proposed learning method with the supervised support vector machine algorithms.

iii. To demonstrate the potential of machine vision application for micro-crack inspection of solar cells.

1.4 Research scope

Due to the different types of crystalline used in the manufacturing process, the multicrystalline solar cell contains many types of defects and deficiencies. All of these

defects are clearly visible in the EL images. One of them is a micro-crack defect which contributed to the electrical failure of the cell. As described earlier, the detection of micro-crack defect is a challenging process due to the presence of other defects in the EL images. Therefore, the scope of this research is limited to the detection of micro-crack defect in the EL images of multicrystalline solar cells. Based on the abovementioned objectives, the algorithm will be developed to distinguish between cracked and intact cell automatically.

1.5 Thesis outline

This thesis is divided into five chapters. In addition to this chapter, Chapter 2 includes the review of the related works in the image processing and machine learning approaches. The review extends to several machine vision-based applications for crack detection. On the other hand, Chapter 3 describes the methodology and experimental procedure implemented in this research. In this chapter, the details of the proposed image processing algorithm and machine learning techniques are also presented. Experimental results of image processing and classification are presented in the Chapter 4 while Chapter 5 concludes the findings of this research.

CHAPTER 2

LITERATURE REVIEW

In this chapter, the review of the literature on two main fields of research related to the works in this thesis is presented. It covers the fields of image processing and machine learning. In image processing, the important aspects such as image preprocessing and segmentation will be reviewed with emphasize are given to the discussion on the anisotropic diffusion filtering technique. Meanwhile, in machine learning, this review covers the supervised and semi-supervised classification approaches focusing on the utilization of support vector machines and clustering techniques. Several applications related to this work from both fields will also be discussed. Additionally, this review also discusses the shape representation techniques and recent machine vision-based crack detection methods.

2.1 Image Processing

Image processing is a core of any computer or machine vision application in the direction of solving vision-related problems (Shapiro & Stockman, 2001; Malamas *et al.*, 2003). The implementation of an image processing task depends on the difficulties of the application where more complex problems lead to highly complicated solutions. Generally, there are two important procedures used in any image processing task namely preprocessing and segmentation (Sonka *et al.*, 2008). Several aims of the preprocessing procedure are noise filtration, edge detection, enhancement and restoration. These steps can be performed in the spatial domain or in other domain through image transformations. Meanwhile, image segmentation typically involves

thresholding step which divides an image into a few distinct parts (Gonzalez & Woods, 2002). The selection of methods or techniques crucially depends on the type of applications or problems.

2.1.1 Preprocessing

Image preprocessing procedure commonly includes image filtering process and detecting edges. Image filtering aims to reduce the present of unwanted noises and interruptions in the image. It can be done in the spatial domain or in the frequency domain. In spatial domain, the filtering is performed on the input image by convolving it with a specific filter mask. This step is referred to as spatial filtering. On the contrary, filtering in the frequency domain requires an image to be transformed into this domain using a discrete Fourier transform (DFT), then, the spectrum is multiplied with the filter function (Gonzalez & Woods, 2002). The filtered image can be obtained through an inverse transformation. In general, frequency domain filtering can be expressed as follows:

$$\mathcal{F}^{-1}\left[\mathcal{F}\left[I\right] \times H\right] \tag{2.1}$$

where I is an input image, H is a filter function and $\mathcal{F}$ denotes DFT. Among the filtering function usually performed at this step are smoothing and sharpening of an image and also removal of the periodical noises.

Edges are the most important textural properties in an image and thus, it holds great amount of information on image representation and description. Therefore, edge detection procedure is a vital step in image processing that assists advanced image analysis and understanding. The criteria of an excellent edge detection procedure is the ability to detect and localize edges accurately as well as producing a precise

response on the edges (Canny, 1986). Detecting edges in an image typically involves a convolution process with a mask. This mask is a gradient operator usually in the form sub-image in the size of 3×3 pixels. Gradient operator approximates the derivatives of the image using the differences of the gray value between neighboring pixels (Sonka *et al.*, 2008). The convolution process sometimes has to be done more than once because certain gradient operator might have multiple masks to examine few directions of edges in an image. In this case, the detected edges are determined by computing the magnitude of the responses from every convolution process. For example, a typical approach of using Sobel gradient operator involves a convolution process in both horizontal and vertical directions of an image. In most applications, the filtering procedure is used for noise reduction or smoothing process. However, the conventional approach of image smoothing process usually resulting in the blurring of the edges.

2.1.2 Anisotropic diffusion

There is a filtering approach referred to as anisotropic diffusion which is able to smooth image while at the same time retain or preserve edges (Perona & Malik, 1990). The foundation of this approach is the scale-space image filtering technique where the original image is iteratively convolved with a filter of variable scales (Witkin, 1984). In the case of anisotropic diffusion filter, the smoothing is a diffusive process where the image is iteratively convolved with a nonlinear filter over a predefined number of times. General anisotropic diffusion model can be mathematically expressed as follow:

$$\frac{\partial}{\partial t} I(m, n, t) = \operatorname{div}\left(c\left(|\nabla I|\right) \nabla I\right) \tag{2.2}$$

where t is iteration, c is the diffusion coefficient, ∇ is gradient and div represents divergence operator. The diffusion coefficient, c, is a function of magnitude of gradient, $|\nabla I|$ and edge stopping threshold, K. The magnitude of gradient is computed for every direction of four nearest neighborhood pixels resembling a Laplacian operator. In this anisotropic diffusion model, the value of the diffusion coefficient varied in the range of 0 to 1 reflecting the degree of the diffusion process and it is monotonically decreased with respect to the magnitude of gradient. Smaller magnitude of gradient yields higher values of diffusion coefficient and thus, produces a strong smoothing effect to the particular pixel. Conversely, the diffusive effect is less when the value of the magnitude of gradient is high and subsequently retains the contrast structure of the particular pixel. The implementation of an anisotropic diffusion filter can be defined in terms of the diffused image, I_D, at iteration t. Mathematically,

$$I_D(m,n,t) = I_D(m,n,t-1) + \frac{1}{4}\sum_{i=1}^{4} c\left(\left|\nabla I_D^i\right|\right)\nabla I_D^i,\ t > 0 \tag{2.3}$$

where c is a diffusion coefficient that is a non-negative function of the magnitude of the gradient of four Laplacian neighbors, $i = \{1,2,3,4\}$. Figure 2.1 shows the Laplacian neighbors for the pixel of interest at coordinate (m,n).

These neighbors are used in the computation of the gradient for the diffusion

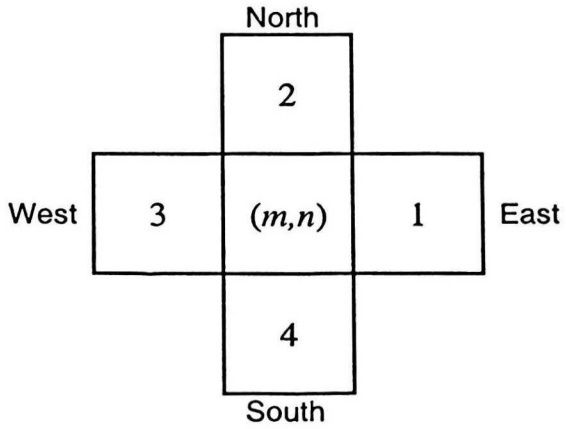

Figure 2.1: Laplacian neighbors of pixel (m,n).

coefficients in Equation (2.3). Mathematically,

$$\nabla I_D^1 = I_D(m,n) - I_D(m,n+1) \tag{2.4}$$

$$\nabla I_D^2 = I_D(m,n) - I_D(m+1,n) \tag{2.5}$$

$$\nabla I_D^3 = I_D(m,n) - I_D(m,n-1) \tag{2.6}$$

$$\nabla I_D^4 = I_D(m,n) - I_D(m-1,n) \tag{2.7}$$

Letting $s = |\nabla I_D|$, the diffusion coefficient originally proposed by Perona and Malik (1990) which is to be used in Equation (2.3) is given as

$$c(s) = \exp\left[-\left(\frac{s}{K}\right)^2\right] \tag{2.8}$$

or

$$c(s) = \left[1 + \left(\frac{s}{K}\right)^2\right]^{-1} \tag{2.9}$$

These diffusion coefficients exhibit a low value at high gradient purposely to preserve the corresponding edges. On the other hand, they produce high value at low gradient indicating a strong smoothing effect on the pixels involved. Thus, the anisotropic diffusion filtering will produce a smoothed image while the important edges are preserved. Parameter K appearing in Equations (2.8) and (2.9) is an edge stopping threshold and it needs to be correctly specified in order to ensure a successful application of this filtering strategy. If K is too small then the diffusion process will be terminated earlier and resulting in $I_D(m,n,t)$ which is approximately equals to $I_D(m,n,0)$. In contrast, fixing K too large will significantly diffuse the image, resulting in image blurring. Therefore, the choice of parameter K is important for producing a diffused image that retains the important edges while smoothing the other regions of the image.

Basically, anisotropic diffusion filter will smooth pixels with the magnitude of gradient less than edge stopping threshold or retain it if otherwise. In practical, the edge stopping threshold is fixed experimentally and most of the case it is highly dependent on the textural properties of an input image. As an example, Figure 2.2(d) shows an output image that has been processed with anisotropic diffusion filter. Comparing this image with the filtered image shown in Figure 2.2(b), it can be observed that the diffused image is smoothed but the edge details are preserved. Furthermore, it can be seen that the locality of most of the preserved edge details in the diffused image are in agreement with the edges shown in Figure 2.2(c).

Since the introduction of the anisotropic diffusion filter by Perona and Malik (1990), considerable amounts of research have been done to date. In the early years, the main focus of the researchers are on the mathematical properties and the understanding of the diffusion model framework as well as its practicality in the application of image enhancement, noise reduction, edge detection and segmentation. Shortly after its introduction, a study on the original diffusion model and coefficients found that it may produce diverging solutions to the images with a very high similarity (Catté *et al.*, 1992). Therefore, in order to overcome this problem, the gradient of the image is

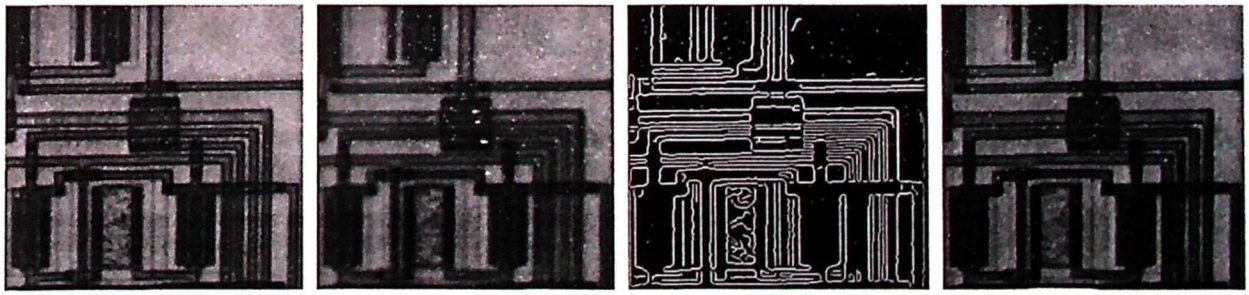

(a) (b) (c) (d)

Figure 2.2: Example of image preprocessing. (a) original circuit image; (b) filtered with Gaussian low pass filter mask of size 5 and standard deviation 3; (c) edge detection using Canny detector; (d) processed using anisotropic diffusion filter with $K = 3$ and $t = 32$.

convolved with low pass filter mask before the diffusion process begins. Meanwhile, the behavioral analysis of the anisotropic diffusion model has been performed in the scope of the optimization problem (You *et al.*, 1996). The conditions of unique solution to the energy function minimization problem have been identified and used to develop the related well-posed and stable model of the diffusion process.

The relation between robust statistics and anisotropic diffusion model has been investigated and the outcome demonstrated few practical benefits (Black *et al.*, 1998). Among them is the estimation of the edge stopping threshold using a robust statistical method known as median absolute deviation (MAD). This estimation approach improves the diffusion process as more edges are preserved in the output image. Meanwhile, an image enhancement strategy using multi-grid approach in anisotropic diffusion has been studied by Acton (1998). The experimental results demonstrated that the computational cost of diffusion process is reduced and low frequency noises are rapidly eliminated. In the other approach, further improvement has been made to the diffusion coefficient such that the transition range of the gradient is preserved even with the variation of edge stopping threshold (Monteil & Beghdadi, 1999). This improvement demonstrated a better noise reduction capability compared to the original approach. However, in estimating the edge stopping threshold, this approach assumes that certain fraction of an image is texturally homogeneous and the presence of noises is independent and identically distributed.

Alternatively, the gradient-based diffusion coefficient defined by function c in Equation (2.2) is replaced with a symmetric positive semi-definite second moment matrix referred to as structure tensor (Weickert, 1999). In this way, the diffusion process is performed mainly in the direction of the highest cohesion in the pixel

contrast. This filtering approach is known as coherence-enhance diffusion (CED) and the results of its implementation have demonstrated a good enhancement of an image with a flow-like patterns. Meanwhile, an anisotropic diffusion filtering technique has been applied in the multi-resolution image analysis for the detection and enhancement of a line structure (Deguchi *et al.*, 2002). The diffusion model in this approach is based on the structure tensor and therefore, produces a non-uniform filtering that enhances the line texture in image.

In another approach, the diffusion process is further developed in order to enhance edges while smoothing through the forward and backward adaptive filtering (Gilboa *et al.*, 2002). In forward diffusion process, the image is smoothed while in the backward diffusion process it sharpens the edges. This approach introduces a set of diffusion coefficients to enable a diffusion process that is adaptively switched from forward to backward mode. Meanwhile, the anisotropic diffusion model is modified by incorporating the critical value function as a diffusion coefficient (Song & Choi, 2004). This function estimates noises in the image based on minimum reliable scale. Through a combination of the function with the local gradient information, the diffusion process enhances the contrast in inhomogeneous regions of an image.

The regularized model of the anisotropic diffusion has been investigated focusing on the implementation of diffusion coefficient (Voci *et al.*, 2004). In this case, an automatic estimation of the edge stopping threshold is proposed to regulate the diffusion model. The estimation using Lyapunov functional of p-norm yields a slow decreasing threshold at each iteration has improved the behavior of the diffusion model. In other approach, the generalizations of the second-order and fourth-order of the anisotropic diffusion model using Euler-Lagrange cost-functional equations have

been proposed (Bai & Feng, 2007). In these generalizations, the diffusion process is performed in the frequency domain and the folded algorithm is applied to the input image to overcome the period boundary conditions of DFT. In comparison with the original implementation, this fractional-order diffusion model was found to be a better approach for noise reduction.

In another approach, the kernel method has been integrated into the anisotropic diffusion model (Yu *et al.*, 2008). In this case, the magnitude of gradient of diffusion coefficient is determined in feature space where the original image is mapped. The outcomes of this approach outperformed the output of conventional diffusion model in simultaneously detecting edges and suppressing noises in an image with low signal to noise ratio (SNR). Meanwhile, an improved anisotropic diffusion model based on image gray level variance has been proposed (Chao & Tsai, 2010). With such improvement, the diffusion coefficient prevents smoothing on the pixels with certain level of variance and subsequently resulting in the diffusion process that preserve important edges and fine details. However, this approach demonstrated an inferior performance on input image that is heavily corrupted or contains multiple impulse noises.

An image noise reduction strategy in pixon domain based on anisotropic diffusion filter has been investigated (Nadernejad *et al.*, 2012). Pixonal image consists of a number of groups of connected pixels in various sizes obtained after smoothing and clustering of an input image in the feature space. A comparative evaluation with several filtering technique shows that this strategy performed well and effective in removing noises. In other application, a context-based anisotropic diffusion has been developed (Li *et al.*, 2012). In this simple approach, the gray level variance is incorporated in

the diffusion coefficient as a weighted factor. Although using similar local image information as Chao and Tsai (2010), this approach has different objective which is noise reduction. On another noise removal strategy, an integration of edge-adapting Laplacian mask in the diffusion model has been investigated (Hajiaboli *et al.*, 2012). The aim of this approach is to overcome the problem of smaller diffusion process on orthogonal edges. This is achieved by reformulating the Laplacian gradient operator (mask) that forced the diffusion process to stop at orthogonal edges. The outcome of this approach has demonstrated a better noise reduction capability in comparison with original diffusion model using conventional Laplacian neighborhood.

Recently, an adaptive anisotropic diffusion model based on edge indicator as a variable exponent has been proposed (Guo *et al.*, 2012). This approach uses an edge indicator to control the filtering strategy on whether to perform a diffusion process or a conventional smoothing operation. Experimental results have indicated that this filtering strategy performed better when compared to other standard filtering techniques. In other approach, the use of an adaptive edge stopping threshold in the anisotropic diffusion model for low contrast image enhancement has been presented (Nafis *et al.*, 2013). The threshold value varied and depends on the statistical information from the gray level histogram of the input image. In this case, the diffusion coefficient is a function of magnitude of the gradient and also local and global variances. The results demonstrated the capability of this approach in preserving the low gray level edges while smoothing the noisy background. Meanwhile, the strategy of choosing the optimal diffusion parameters namely an edge stopping threshold and the number of iteration has been investigated (Tsiotsios & Petrou, 2013). The edge stopping threshold is determined using knee algorithm on the histograms of

the magnitude of directional gradient. In this strategy, two edge stopping thresholds corresponding to the vertical and horizontal gradients are estimated. The experimental results demonstrated that this approach outperforms other conventional diffusion filter in terms of edge preservation and noise suppression. In the case of the number of diffusion iteration, the value is selected if it maximizes the metric that examines the quality of the edges in the image.

The advantages of anisotropic diffusion filter have attracted many researchers in investigating the implementation of this filtering technique in other image processing applications. For example, the applications of anisotropic diffusion filter in the processing of medical images. The implementation of this filtering technique exhibit efficient noise reduction and edge preservation and subsequently, enhance the important structure of the magnetic resonance (MR) image (Gerig *et al.*, 1992). The filter also performed well in preparing MR images for the segmentation process compared to other multi-scale filtering technique (Niessen *et al.*, 1997). Based on robust anisotropic diffusion model by Black *et al.* (1998), the sharp and noiseless statistical parametric maps (SPM) of the functional MR imaging are successfully achieved (Kim *et al.*, 2005). Recently, in the noise removal algorithm for MR images, the similarity index has been used in the determination of the optimal number of diffusion iteration (Ferrari, 2013).

In addition to MR images, anisotropic diffusion filter has also been used in the preprocessing other medical images. A hybrid filtering approach combining anisotropic diffusion with median filter has been proposed in smoothing the low SNR molecular images (Ling & Bovik, 2002). In another application, the anisotropic diffusion filter with modified coefficient has been applied in a preprocessing step of